Northumbria Research Link

Citation: Chen, Jinkai, Xuan, Weipeng, Zhao, Pengfei, Farooq, Umar, Ding, Peng, Yin, Wuliang, Jin, Hao, Wang, Xiaozhi, Fu, Yong Qing, Dong, Shurong and Luo, Jikui (2018) Triboelectric effect based instantaneous self-powered wireless sensing with self-determined identity. Nano Energy, 51. pp. 1-9. ISSN 2211-2855

Published by: Elsevier

URL: https://doi.org/10.1016/j.nanoen.2018.06.029 <https://doi.org/10.1016/j.nanoen.2018.06.029>

This version was downloaded from Northumbria Research Link: http://nrl.northumbria.ac.uk/id/eprint/34512/

Northumbria University has developed Northumbria Research Link (NRL) to enable users to access the University's research output. Copyright © and moral rights for items on NRL are retained by the individual author(s) and/or other copyright owners. Single copies of full items can be reproduced, displayed or performed, and given to third parties in any format or medium for personal research or study, educational, or not-for-profit purposes without prior permission or charge, provided the authors, title and full bibliographic details are given, as well as a hyperlink and/or URL to the original metadata page. The content must not be changed in any way. Full items must not be sold commercially in any format or medium without formal permission of the copyright holder. The full policy is available online: http://nrl.northumbria.ac.uk/policies.html

This document may differ from the final, published version of the research and has been made available online in accordance with publisher policies. To read and/or cite from the published version of the research, please visit the publisher's website (a subscription may be required.)

Northumbria University NEWCASTLE

University Library

Triboelectric effect based instantaneous self-powered wireless sensing with self-determined identity

Jinkai Chen[1, 2], Weipeng Xuan[1], Pengfei Zhao[5], Umar Farooq[2], Peng Ding[2], Wuliang Yin[3], Hao Jin[2], Xiaozhi Wang[2], Yongqing Fu[4], Shurong Dong[2*] and Jikui Luo[1,5*]

1. *Ministry of Education Key Lab. of RF Circuits and Systems, College of Electronics & Information Hangzhou Dianzi University, Hangzhou, China.*
2. *Key Lab. of Adv. Micro/Nano Electron. Dev. & Smart Sys. of Zhejiang, College of Info. Sci. & Electron. Eng., Zhejiang University, Hangzhou, China.*
3. *Sch. of Elec. and Electron. Eng., University of Manchester, Manchester M60 1QD, U.K.*
4. *Faculty of Engineering and Environment, Northumbria University, Newcastle upon Tyne NE1 8ST, UK*
5. *Inst. of Renew. Energy & Environ. Technol., University of Bolton, Deane Road, Bolton BL3 5AB, UK.*

*Email: J.Luo@bolton.ac.uk, dongshurong@zju.edu.cn

Abstract: Sensors are the foundation of modern Internet of Things, artificial intelligent, smart manufacturing *etc*, but most of them require power to operate without spontaneous unique identifiable function. Herein we propose a novel instantaneous force-driven self-powered self-identified wireless sensor based on triboelectric effect to meet the huge demand of true self-powered wireless sensors. The device consists of a microswitch controlled triboelectric nanogenerator (TENG) in parallel with a capacitor-inductor oscillating circuit, and a wireless transmitter. The system is fully powered by the

output of the TENG to generate a resonant frequency containing sensing and device identity information, which is then coupled to the transmitter for realizing a long-range wireless communication. The device, with the multiple functions of energy harvesting, sensing, identity generation and wireless signal transmission, is a standalone device, which responds to each trigger without losing sensing information. It eliminates the requirement of electric components for traditional wireless communication, such as rectification circuit, energy storage units, microprocessor, wireless communication chip, *etc*. Thus, we developed a true self-powered identifiable wireless sensor with great potential for widespread applications.

Keywords: triboelectric nanogenerator, self-powered, self-identified, wireless sensor, resonant circuit.

1. Introduction

Internet of things (IoT), artificial intelligence (AI), smart manufacturing and smart buildings,[1-5] *etc*. are making rapid progress with significant impacts on our daily lives, societies and industries in all aspects. Wireless sensor networks (WSNs) are the most fundamental technologies of these modern concepts, but are faced with two major challenges: power and identification for the large number of sensors in the networks.[6-9] The wireless sensors installed in remote areas or harsh environments need to implement long-term sensing/monitoring tasks,[6-8] which are difficult to be powered by ordinary electricity or to change the batteries periodically. Furthermore, instead of identifying themselves, most of the sensors require additional electronic components to achieve

identities (ID).

Nanogenerators technologies have been explored to power wireless sensors locally by utilizing piezoelectric,[10, 11] pyroelectric,[12, 13] electromagnetic [14, 15] and triboelectric [16-22] effects or a hybrid of these effects[23-29] that harvest energy from ambient environment. However, the existing designs typically require rectifier and energy storage units to store the electric power, subsequently regulate the voltage to power the wireless sensor chip with a very low power conversion efficiency. On the other hand, current wireless communication chips require a high power to operate, in the order of several milli-watts though in a short period of time, with which the nanogenerators are typically unable to meet. To fulfil the power demand for the wireless sensor chip(s), the nanogenerator embedded in the systems need to work for a relatively long period of time before the transmission process which results in severe information loss, particularly if the nanogenerator does the sensing function simultaneously. Although the sensor ID issue can be solved by integrating radio frequency ID (RFID) on the chip,[30] or using surface acoustic wave sensors which can integrate IDs in the sensors,[31, 32] the ID information can only be obtained through passive triggering.

Here we report an instantaneous self-powered self-identified wireless sensor device based on triboelectric effect. The device can generate electricity to power itself, perform sensing, produce identity and realise the wireless transmission of the complete information simultaneously for each force triggering action. To elucidate this innovative sensor device, we will introduce the concept and structural evolution of the development from the triboelectric nanogenerator (TENG), resonant circuit design, wireless transmission, and sensing performance in the

following sections.

2. Methods

2.1 TENG fabrication

Glass and PDMS were used as the triboelectric materials to make the TENG for demonstration. The PDMS (184 Silicone Elastomer, Dow corning Co. Ltd.) solution, which is a mixture of the base PDMS and the cure agent at a ratio of 10:1 by mass, was spin-coated on the clean side of an Al adhesive tape at 1100 rpm for 10 sec to obtain a PDMS thin film with a thickness of ~100 μm, and was glued on the surface of a commercial acrylic support layer. The PDMS layer on the Al tape was cross-linked on a hot plate at 100 °C for 25 min. The glass part consists of a commercial soda lime glass of 1 mm thickness, a double-side conductive nickel adhesive tape and a 2 mm glass support layer. For the TENG with the microswitch, the PDMS part is same as mentioned above, while the 2 mm glass support layer was replaced with a switch structure.

2.2 Microswitch fabrication

The microswitch consists of two acrylic support layers linked with 4 springs at the corners of the acrylic plates. The outer diameter, inner diameter, free length and the spring constant of the spring is 8 mm, 4 mm, 50 mm and 0.35 Kgf/mm, respectively. A z-axis translation stage with an Al adhesive tape on the surface was fixed at the bottom of the acrylic support layer to control the distance, z, between the Al electrode on the upper and the lower acrylic layers. The resolution for the z distance control is ~10 μm.

2.3 TENG measurement setup

A dynamic fatigue tester (Popwill Model YPS-1) was utilized to control the cyclic contact force, frequency and distance. The voltage and current outputs were obtained using an oscilloscope (LeCroy WaveSurfer 104 Xs) and a picometer (Keysight B2981A), respectively. The inductor for transferring energy wound on a plastic core with a 5 mm diameter. The electric output of the TENG sensor was connected to a commercial 650 nm laser diode with a 3.3 V threshold voltage and 5 mW rated power. The capacitance, inductance and resistance of testing probe was tested using LCR meter (TONGHUI electronics TH2828). A commercial Si photodiode (Hamamatsu s5971) and a trans-impedance amplifier (FEMTO DHPCA-100) were used to collect and subsequently amplify the optical signal received.

3. Results

Figure 1a shows the concept/schematic diagram of the instantaneous self-powered self-identified wireless sensor device. It consists of a triboelectric nanogenerator integrated with a micro-mechanical switch (microswitch), an LC resonant circuit, and a coupling inductor connected to a transmitter. A remote responsive receiver is used to receive the sensing information with identity sent by the transmitter wirelessly. In this work, a red laser and a photodetector were used as the transmitter and receiver, respectively, for the wireless communication demonstration; the communication method can be expanded to utilise radio-frequency technique with a proper antenna in the future work. When the TENG is pressed

(triggered) by an external force caused by mechanical vibration, wind, *etc*., it will produce a pulsed high voltage output controlled by the synchronized microswitch. The voltage output is coupled into the LC resonant circuit to produce a damping resonance with sensing information contained and a fixed frequency. The resonant signals are further coupled to the transmitter through an inductor to transmit to the remote receiver. The received signals are analysed for sensing information, subsequently processed to obtain resonant frequency for the identity of the sensor by a fast Fourier transform (FFT) algorithm. Continuous triggerings produce a series of pulsed voltage outputs, leading subsequent series responsive resonant and transmitting signals, to realise a true self-powered wireless sensing process with identity attached without any information loss.

The TENG used for this demonstration has a dimension of 4.5×4.5 cm^2, consists of a glass positive triboelectric plate (~1 mm thickness) and a polydimethylsiloxane (PDMS) negative triboelectric plate (~100 μm thickness). An aluminium (Al) conductive tape (for PDMS) and a double-side nickel conductive tape (for glass) were attached on the backside of corresponding plates as the electrodes. To simulate the situation that two spaced plates contact with each other by external forces, the glass plate moves up and down to make contacts with the PDMS surface during the experiments by utilizing a fatigue tester system. Additional fabrication process of the TENG can be found in the Methods section.

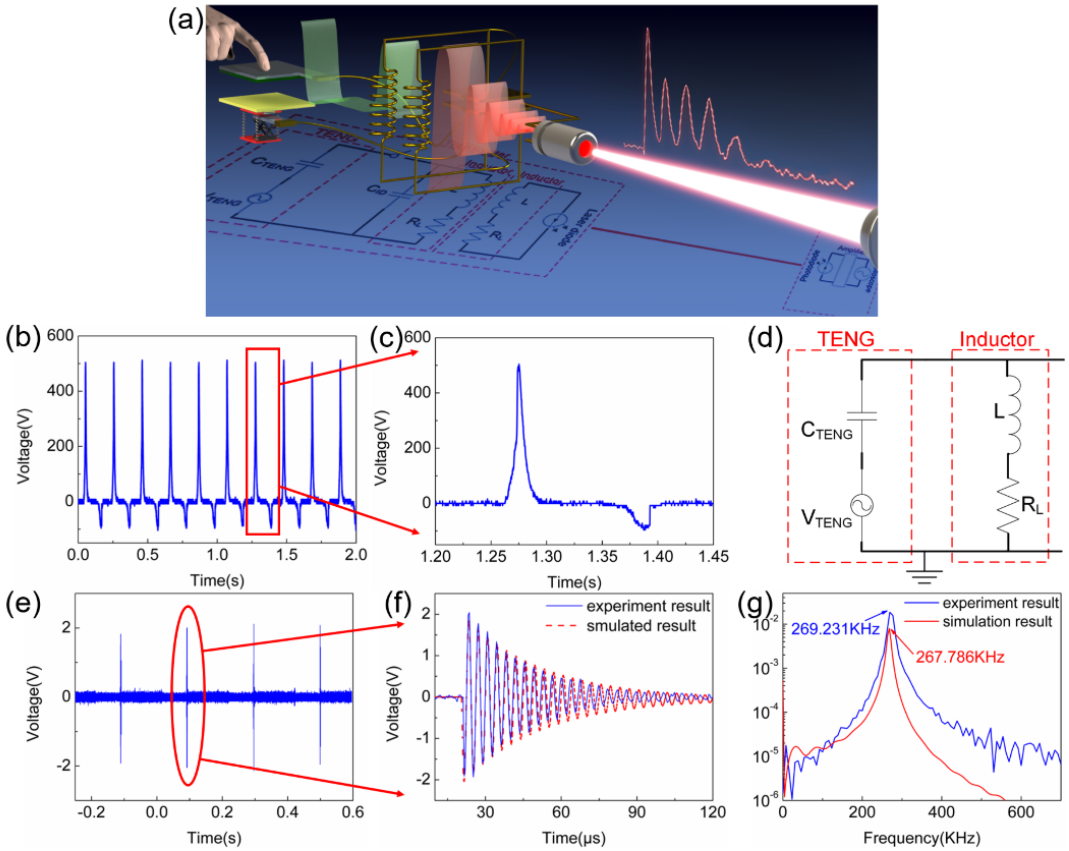

Fig. 1. Schematic and results of the self-powered self-identified wireless sensor. (a) Schematic drawing of the instantaneously self-powered wireless sensors with identity, (b) typical voltage output of a contact-separation mode TENG under cyclic pressing of an external force, (c) zoomed-in pulse output voltage, (d) the equivalent resonant circuit of the TENG sensor with an external inductor, (e) a series resonant signal produced by the resonant circuit when the series output voltages of (b) are coupled into the inductor with details of one impulse shown in (f), the signal oscillates with a damping factor determined by the inherited resistance of the inductor, and the resonant spectrum (g) obtained by Fast Fourier transformation with a fixed resonant frequency.

3.1 Functions of the microswitch

For the vertical contact-separation mode TENG, contact layers typically consists of two insulator

membranes with very different electron affinities, i.e. one tends to lose electrons (called positive tribo-material hereafter) and one tends to accept electrons (called negative tribo-material). Conductive electrodes are fabricated on the back of the contact layers and connected to a load to form a closed circuit. When the TENG is pressed by a triggering force, the two separated insulator layers make a contact and tribo-charges are produced on the surfaces of layers with opposite polarities. After the triggering force is released, an induced electric potential is generated between the backsides of the two electrodes and increases with the increase of the separation until two layers are restored to the initial position, resulting in one cyclic voltage output. The cyclic open-circuit voltage (V_{oc}) output produced by the TENG is shown in Fig. 1b.

Theoretical analysis has been conducted by a number of researchers,[33-36] and the characteristics of the contact-separation mode TENGs are well re-produced. Theoretically, the vertical contact-separation mode TENG can be considered as a capacitor, C_{TENG}, connected with a voltage source, V_{TENG}, in series. They can be expressed by the following equation:[36]

$$V_{TENG} = \frac{\sigma x(t)}{\varepsilon_0} \tag{1}$$

$$C_{TENG} = \frac{\varepsilon_0 S}{d_0 + x(t)} \tag{2}$$

Where σ, $x(t)$, ε_0 and S represent the surface charge density, distance between two tribo-plates over time, vacuum permittivity and contact area, respectively. d_0 is the effective thickness of the TENG, and is defined as

$$d_0 = \frac{d_1}{\varepsilon_{r1}} + \frac{d_2}{\varepsilon_{r2}} \tag{3}$$

Where d_1 and d_2 are the thickness, ε_{r1} and ε_{r2} are the relative permittivity of the upper and lower triboelectric membranes, respectively.

By connecting the TENG with an inductor, it forms an RLC resonant circuit (the equivalent circuit is shown in Fig. 1d), where the inductor has a resistance, R_L. The voltage output from the TENG provides the impulse electricity to the resonant circuit for oscillation, and produces a damping resonant signal at the two terminals of the inductor with a resonant frequency, f_r, determined approximately by

$$f_r = \frac{1}{2\pi\sqrt{LC_{TENG}}} \tag{4}$$

where L is the inductance of the inductor. For the RLC circuit, the damping factor ζ determines the type of transient state which can be expressed as

$$\zeta = \frac{R_L}{2}\sqrt{\frac{C_{TENG}}{L}} \tag{5}$$

Fig. 1e shows the resonant signals measured from the two terminals of the inductor (L = 2.13 mH), and Fig. 1f is one of the zoomed-in damping oscillating signal.

TENGs normally have very large output impedance in the range from tens of mega-ohms to a giga-ohms,[34, 37, 38] while inductors have extremely small input impedance, ranging from a few ohms to a few hundreds of ohms depending on the inductance and material used. Thus, the output voltage of the TENG can not be coupled to the inductor effectively when the inductor is directly connected to the TENG. Furthermore, the signal width shrinks significantly from typical tens of milliseconds to microseconds in this near-short-circuit situation. In such situation, the resonant signal produced by the RLC circuit is very weak due to the limited energy coupled in,

apparently insufficient for long distance wireless communication. Fig. 1f shows the oscillating voltage output coupled to the inductor with the maximum amplitude of V_{P-P} ~4 V (peak-to-peak voltage) with a narrow damping signal period (~100 μs), even though the peak V_{oc} values of the TENG is over 500 V. The red dashed line in Fig. 1f illustrates the simulated result modelled based on SPICE software with the actual device and operation parameters as the input data, and Fig. 1g compares the frequency spectrum transformed from the experiment and simulated time-domain results in Fig. 1f, which shows an excellent agreement with the experimental resonant result, indicating the valid of the equivalent circuit and TENG model. Detailed modelling and parameters used can be found in SI. It is worthy to mention that when a probe and an oscilloscope are connected to measure the oscillating signal in parallel to the inductor as shown in Fig. S1, they will influence the detected results because of the finite input impedances. The equivalent circuit is shown in Fig. S1, implying the results shown here are influenced, resulting in a slight difference from that of the actual circuit situation.

To solve the mentioned issue, we introduced a microswitch into the TENG, which is capable to synchronize with the movement of the TENG operation, to produce large instantaneous power output and to stabilise the resonant frequency. The structural demonstration of the microswitch (not in scale) is shown in Fig. 2a circulated by the red dotted line which has a similar operational concept to those reported articles.[39, 40]

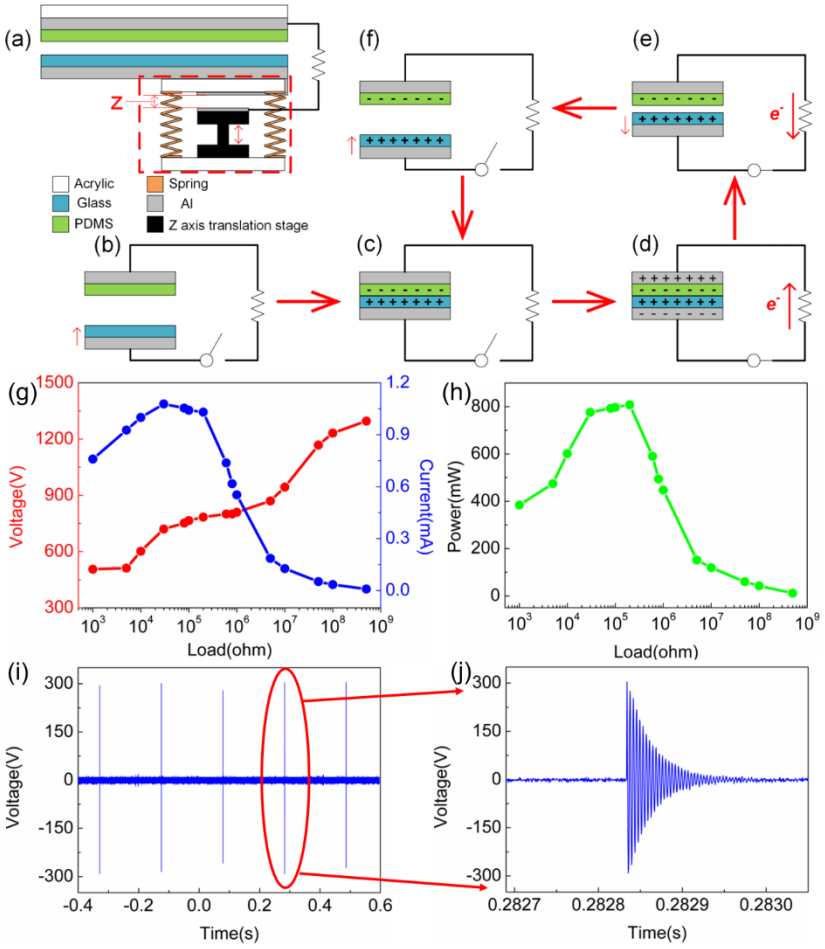

Fig. 2. Microswitch and its effect on the outputs of the TENG. (a) Schematic of the TENG and microswitch, (b-f) show the synchronized movement of the microswitch with the movement of the TENG lower plate, (g) and (h) are the output voltage, current and power as a function of the load resistance for the TENG with the microswitch. The outputs have been enhanced significantly with the power output increased to 800 mW, and (i-j) the resonant signal coupled into the resonant circuit and one zoomed-in pulse output voltage. The peak-to-peak amplitude of the resonant signal increases from ~4 V to ~600 V once the microswitch and a resonant capacitor are connected, sufficient to drive wireless transmitter part of the circuit.

The microswitch consists of two parts, four springs for ensuring an off-state and a z-axis

translation stage, which can control the distance z between the lower working electrode fixed on the transition stage and the electrode attached on the bottom triboelectric contact layer. The upper contact layer remains fixed and the lower glass plate with the microswitch is driven by external force from the bottom acrylic layer. The operation principle of the TENG with the microswitch is shown in Fig. 2b-2f. Initially, there is no charge inducted in the upper and lower triboelectric materials, and the switch is at the off-state. Subsequently, as shown in Fig. 2c, the glass layer begins to move upwards by an external force until it is contacted with the PDMS surface while the springs set on the microswitch are not being compressed (microswitch state: off). The inductive charges cannot be discharged and will accumulate in the electrodes. With further rise of the glass layer as shown in Fig. 2d, the springs are compressed until the electrode fixed on the translation stage contacts with the back electrode of the glass layer (microswitch state: on), leading to an instantaneous flow of the whole accumulated charges to the circuit. Finally, the glass layer starts to move downwards (Fig. 2e), and then microswitch is at off state (Fig. 2f) until the glass layer reaches the lowest position to complete one energy generation/sensing cycle.

The accumulation and instantaneous discharge of inductive charges by using microswitch will greatly increase the electric performance of the TENG, which is shown in Figs. 2g-2h tested under the conditions of 50 N contact force, 5 Hz working frequency, 4 mm separation distance and 0.9 mm z distance. It can be seen from Fig. 2g that the voltage output increases from 506 V to 1296 V along with the external load increases from 1 kΩ to 900 MΩ. In the meantime, the current output increases from 8.74 μA at 900 MΩ to 1.08 mA at 30 kΩ, then it slowly decreases to 759 μA at 1 kΩ. The downward trend in Fig. 2g looks different from the typical current curves

when the external load is decreased from 30 kΩ to 1 kΩ. The reason is as flows: the signal width shrinks significantly when the external load becomes smaller. As the fastest sampling rate of the picoammeter is 10 μs/point, we can easily acquire an accurate current curve and peak value when the external load is 100 MΩ, while we can only acquire a very rough current curve when the external load is 1 kΩ. The decreasing current output when the external load is smaller than 30 kΩ is resulted from the shrunk signal width of the TENG output which cannot be fully acquired by the picoammeter with the fastest sampling rate of 10 μs/point. An in-depth exploration about this phenomena will be carried out when a new current measuring equipment is purchased in the future. The detailed discussion can be found in Fig. S3. According to previous researches based on a similar switch function, the actual outputs could be much larger than the measured results at low external load.[39, 40] However, even based on the measured results, as shown in Fig. 2h, the maximum output power reaches 808 mW at a 200 kΩ external load. In contrast, according to our previous research, the maximum power output for the same TENG without the microswitch is ~1.5 mW with a larger independent resistance of ~40 MΩ.[34] It is clear that the microswitch can not only boost the instantaneous electric output of TENGs, but also reduce the output impedance of the TENG dramatically. The greatly enhanced instantaneous outputs of the TENG are attributed to the much-shortened charge release time from milliseconds to microseconds for the accumulated charges through the microswitch. With such high instantaneous power output and low output impedance, the TENG with the microswitch is expected to produce strong oscillating signal when it is coupled to an inductor directly. Fig. 2i represents the resonant signals from the resonant circuit with an external identity capacitor C_{ID} (C_{ID} function will be discussed in

the following section), which was triggered by a series of external force. As it is shown in Fig. 2j, the peak-to-peak voltage amplitude of the oscillating signal increases by two orders of magnitudes, from ~4 V (without microswitch) to ~600 V, without changing the damping characteristics.

As discussed above, TENG can be considered as a capacitor (C_{TENG}) connected with a voltage source (V_{TENG}) in series, and, theoretically, the TENG capacitance C_{TENG} is significantly affected by displacement x(t) of the two triboelectric materials. It is suitable to generate a resonant signal with accurate identity information by using C_{TENG} as it can be influenced by working conditions which is related to the value of x(t) or the movement trace of the moving tribo-plate, such as the acceleration of the contact layers, working frequency, space distance between the triboelectric materials, *etc*. Detailed discussion of the influences is shown in Fig. S3. Before introducing the microswitch into the system, for generating an identified resonate signal, an identity capacitor (C_{ID}) is connected in parallel to the TENG. The resonant frequency of this circuit is as follows,

$$f_{ID} = \frac{1}{2\pi\sqrt{L\left(C_{TENG} + C_{ID}\right)}} \tag{6}$$

It is expected to generate a resonant signal with less influence from the variation of the TENG capacitor by using a C_{ID} with larger capacitance than C_{TENG}. Figs. 3c-3e illustrate the resonant frequencies generated by the resonant circuit with C_{ID} of 195 pF and inductance of 2.13 mH under different contact conditions (frequency, force and distance). The resonant frequencies for the device are roughly determined to be ~175 kHz with a large fluctuate of approximately

±10 kHz, which is apparently not stable enough to be used as the identity for the TENG sensor. However, after introducing the microswitch into the device, as shown in Fig. 3b, the resonant frequency generated by the sensor is no longer affected by the operation conditions of the TENG. When the microswitch is at the on state, it couples the power to the resonant circuit to generate oscillating signal, the relative displacement x(t) of two triboelectric materials remains zero as they have already contacted until the microswitch is off, thus the C'_{TENG} is a constant, and is given by

$$C'_{TENG} = \frac{\varepsilon_0 S}{d_0} \tag{7}$$

Thus, the generated resonant f_{ID} will be determined largely by the C_{ID} capacitor and is a constant, not influenced by the working conditions *etc*. The resonant frequencies using 195 pF C_{ID} under different contact conditions (frequencies, forces and distance) are shown in Fig. 3f-3h. They remain constant within a negligible experimental error range of 2 kHz. Thus, it is reasonable to use C_{ID} as the identity tag for the wireless signal transmission.

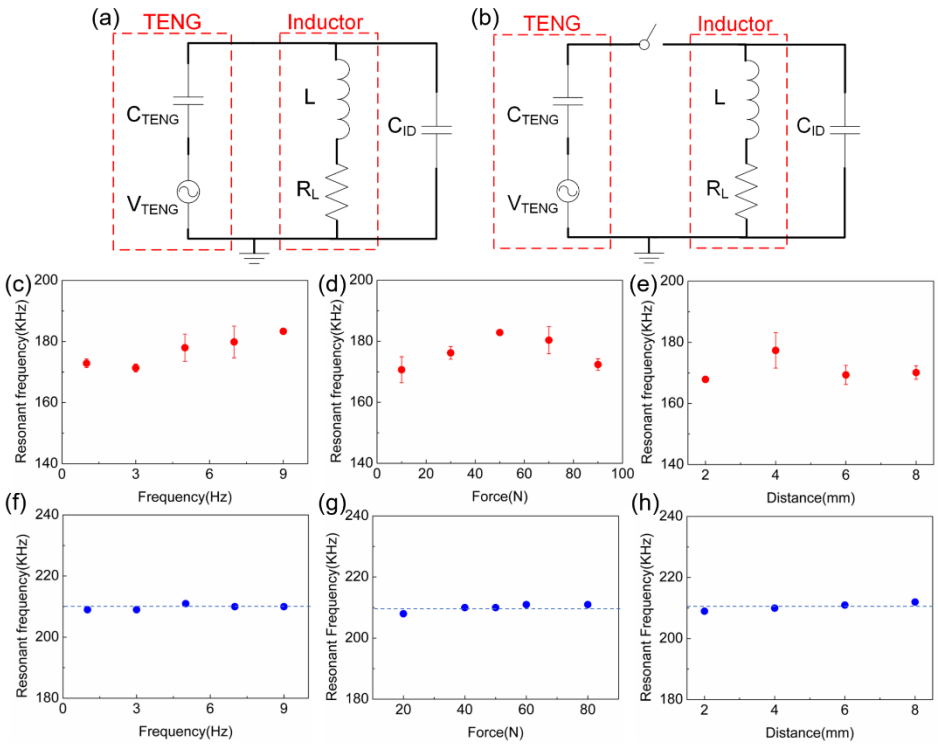

Fig. 3. Stability enhancement of identity resonant frequency by using an external capacitor C_{ID} and a microswitch. TENG oscillating circuit with an external capacitor with (a) and without (b) microswitch function to stabilise the resonant frequency. The resonant frequency for the circuit without identity capacitor and microswitch as a function of contact frequency (c), force (d), and distance (e), or with an identity capacitor and a microswitch as a function of contact frequency (f), force (g), and distance (i).

3.2 Resonant circuit and identity

To investigate the relationship of resonant frequency with C_{ID} capacitor and resonant inductor, Fig. 4a shows the comparison of the resonant frequencies detected from practical experiment with the corresponding theoretical analysis results. Due to the lack of the microswitch model in SPICE software, a brief calculation based on equation (6) with a constant C_{TENG} based on equation (7) ($S=4.5\times4.5$ cm^2) was carried out, which are represented as the solid lines in Fig. 4a.

For all inductances and capacitances, the measured resonant frequencies are in agreement well with the theoretical results, indicating the valid of the model. The results also indicate the capability of the identity capacitor for generating accurate and predictable identity.

Fig. 4b shows the standard deviation of resonant frequency of multiple contact tests with different C_{ID}s. The baseline resonant frequencies are 476 kHz, 264 kHz, 210 kHz, 177 kHz and 156 kHz for C_{ID}= 0, 112, 195, 336 and 451 pF, respectively. The standard deviation drops with the increase of capacitance of C_{ID}. Based on the standard deviation of frequency and values of C_{ID}, the whole amount of available identity tags can be approximately estimated. As the standard deviation decreases with increasing identity capacitance, the frequency interval can be set to be 2 kHz, 1.5 kHz, 1.5 kHz and 1.0 kHz for the frequency bands of 476-264 kHz, 264 kHz-210 kHz, 210 kHz-177 kHz and 177 kHz-156 kHz, respectively. Thus, the total number of identity tags can be estimated to be 186. It is worthy to mention that the resolution of 1 kHz obtained from the FFT analysis was used for the calculation, which is actually much larger than most of the standard deviations, therefore, a larger amount of available identity tags can be set by using frequency spectra with a higher resolution.

The transient state of an RLC circuit is determined by the damping factor as given by Equation (5). A desired underdamped response could be generated when the damping factor ζ is smaller than 1. For example, an inductor with an inductance of 2.13 mH and resistance of 80 Ω, connected to a capacitor with a capacitance smaller than 1.33 μF, an underdamped response will be generated, corresponding to an identity tag with a resonant frequency of 2.99 kHz. As the above discussion attests, the total number of available identity tags could be much more than we

have calculated.

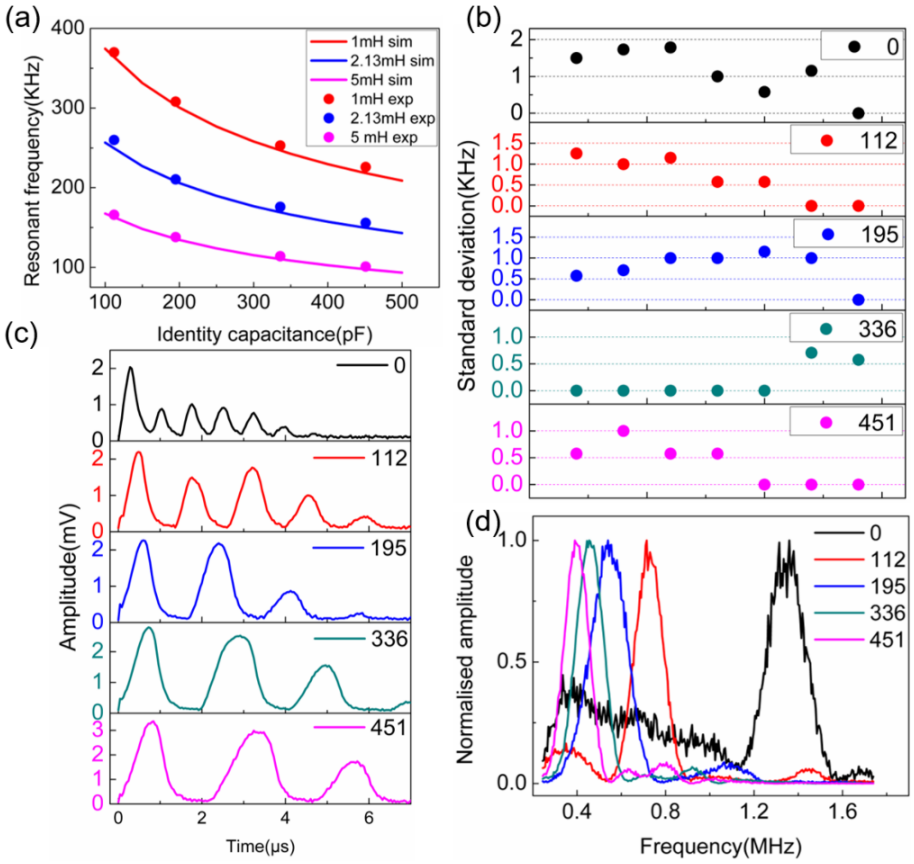

Fig. 4. Design and measurement of identity resonant frequency for the self-powered wireless sensors. (a) Comparison of resonant frequency as a function of identity capacitance and inductance, the resonant circuit with stable identity frequency under 20 N force, 5 Hz contact frequency and 4 mm distance between the two tribo-layers, (b) output signals from the remote receivers with identity and sensing information contained, (c) received signals with different C_{ID}s from the transmitter by the photodetector, and (d) the normalized FFT spectrum as a function of the identity capacitance.

Fig. 4c shows the damping resonant signals received by the remote photodetector as a function of C_{ID} capacitance varying from 0 pF to 451 pF, combined with a 454 μH inductor. The

TENG outputs were generated at the conditions of 20 N force, 5 Hz contact frequency and 4 mm distance between the two tribo-layers. It is clear that the response times is usually smaller than 7 μs when C_{ID}=451 pF is used, and it gradually decreases to ~4 μs when there is no identity capacitor used. The maximum resonant frequency for the sensor is 1.4 MHz (C_{ID}=0) as shown in Fig. 4d, and the minimum frequency is ~100 kHz when a 5 mH inductor is used (Fig. 4a). The maximal allowed bandwidth of the TENG sensor is therefore, about 1.3 MHz, but it would be reduced significantly when considering all other parasitic factors, the ID number and transmission requirement, and design margins for each resonant peak. The amplitudes of the detected resonant frequencies decline with the raise of capacitance monotonically. They were further analysed by FFT to extract the resonant frequency (Fig. 4d). The resonant frequency increases from 400 kHz to 1.35 MHz with the capacitance of C_{ID} varied from 0 pF to 451 pF. The resonant frequency fluctuation from the signal with 451 pF C_{ID} is much smaller than that from the signal with 0 pF capacitor, demonstrating the stabilization effect of a large identity capacitor as expected. Besides, it can be seen from Fig. 4c that the output amplitude increases slightly when the C_{ID} increases from 0 pF to 451 pF. As we all know, for an RLC resonant circuit, the largest output amplitude occurs when the frequency of the signal source (TENG) is the same as the resonant frequency of the total RLC circuit, and the output amplitude will decrease when these two frequencies are different. The typical pulse width of the microswitch integrated TENG under the near short-circuit load is around 50 microseconds, so the frequency of the signal source (TENG) can be considered smaller than 50 kHz, while the resonant frequency of the total RLC circuit, which can be seen in Fig. 4d, varies from 400 kHz (C_{ID}=451 pF) to 1.35 MHz (C_{ID}=0 pF),

which means the frequency of the signal source (TENG) is smaller than the resonant frequency of the total RLC circuit. Therefore, increase of C_{ID} will lead to a decrease of the resonant frequency of the total RLC circuit more approaching to the frequency of the signal source (TENG), which results in a slightly larger output. If the output amplitude is considered to be the sensing information, calibrations should be carried out for the TENG wireless output signals with different identity tags for a more accurate sensing result.

3.3 Wireless communication and sensing:

Owing to the integrated microswitch and identity capacitor, large-magnitude damping oscillation signal embedded with identity information (Fig. 2j) can be generated when the TENG sensor is driven by external forces. To demonstrate if the device is able to drive a transmitter for wireless communication, a red laser was used to perform a practical wireless test. The final design of the device is shown in Fig. 5a. By using a coupling inductor, the generated resonant signals are coupled to the transmitter inductively without losing the sensing (magnitude) and identity (frequency) information. On the other hand, a commercial photodiode for detecting wireless signal from the laser diode, a trans-impedance amplifier (TIA) for converting the current signal to voltage signal and a data acquisition device (an oscilloscope) were connected together as the receiver side (detailed information in Methods section). The test wireless transmitting range was set to be three meters, which was restricted by the space of the laboratory. Owing to the ultra-strong signal output of the laser diode attributed to the enhanced resonant signal generated by the circuit, the receiver can easily detect both the sensing signals and the identity tag at the

distance with the indoor light switched on. The laser beam of the diode was aligned with the receiver by manual adjustment due to the limitation of the laboratory condition, and the wireless transmission distance can be enhanced dramatically if the laser beam is aligned and focused by precision adjustment and by using lens. A video (Movie. S1) of the laser light transmission under operation can be found in the SI, showing the real-time transmission of the information.

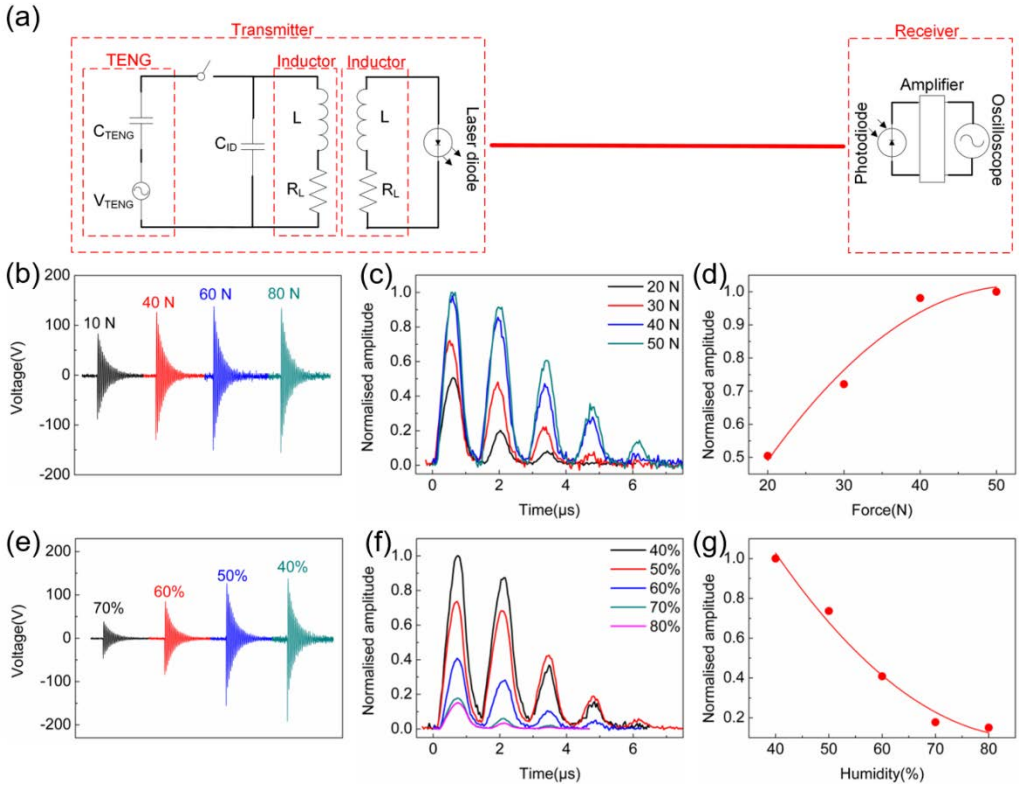

Fig. 5. Wireless sensing by the self-powered self-identified TENG sensor. (a) the equivalent circuit of the wireless sensor with a laser as the transmitter. (b) and (e) the oscillating signals generated under different contact forces and humidity measured from the two terminals of the inductor. (c) and (f) the normalized variation of the amplitude with contact force and humidity, received by the photo-detector from the laser located 3 meters away, demonstrating its ability to perform the remote wireless sensing by the TENG sensor with identity. The sensor is able to sense wirelessly once it is triggered, thus no any

information is lost.

The received sensing signals and the FFT spectra from the laser transmitter with different C_{ID}s are shown in Figs. 4c-4d. Since the signal can only pass the diode through one direction, the received signal was rectified to be a DC signal. However, the procedure does not affect the transmission of the retained resonant information.

Although the resonant frequency of the signal is determined by the C_{ID}, the amplitude of the oscillating signals was found to be correlated with operation conditions. This feature can be utilised as a sensing function. The signals generated by the device when the TENG is operated under different contact forces/humidity levels are shown in Figs. 5b-5g. Both the resonant inductor and the coupling inductor for the laser have an identical inductance of 454 μH, with a resistance of 23 Ω. The amplitude of the received oscillating signal was found to increase with the contact force when it is smaller than 40 N, and remain constant with further increase in force, consistent with the direct measurement from the oscillating circuit of the TENG (Fig. 5b). On the other hand, the amplitude of the received resonant signal decreases rapidly with the increase in humidity level from RH40% to RH70%. The amplitude change of the received resonant signal from the sensor is attributed to the increase in surface conductivity of the triboelectric material surfaces when humidity increases, which will enhance the leakage of charges generated by triboelectric induction.[41] Based on the tested results shown above, it is reasonable to expect the device to be used as a sensor to realise the long-range transmission of the force/humanity data wirelessly based on the magnitude of the transmitted resonant signal.

4. Conclusion

In summary, we proposed a novel triboelectric effect based instantaneous self-powered self-identified wireless sensor. The device consists of a TENG sensor, an identity capacitor-inductor oscillating circuit, a wireless transmitter, and a remote receiver for signal receiving and processing. By integrating a micromechanical switch into the TENG, the instantaneous outputs of TENG have been enhanced significantly with a maximum V_{p-p} and power up to ~1296 V and ~808 mW with a significant reduced output impedance. It was also found that the microswitch is capable to stabilise the capacitance of the TENG. When the output of the TENG is coupled to the RLC resonant circuit, it produces oscillating signal with a V_{p-p} up to 600 V and a constant resonant frequency, used as a wireless identity tag, which is strong enough to be transmitted wirelessly to the remote receiver for processing through a transmitter. This novel device with the functions of energy harvesting, sensing, identity tag generation and wireless signal transmission can transmit signal wirelessly for 3 meters with potential for great improvement in transmission distance. We also demonstrated the wireless sensing capability for sensing humidity and force using this device. The sensor is a standalone device, responds to every trigger without losing any sensing information and does not need any external electric power supplier, rectification circuit, energy storage units, microprocessor, wireless communication *etc* electronics, and is a true self-powered wireless sensor with identity and has great potential for widespread applications. Potential applications of this novel self-powered, self-identified wireless sensors is broad, such as security, anti-thieves, anti-intruders,

head-counting, health monitoring for infrastructures or public transportation like bridges, buildings, and for public transportation such as trains, railways.

Supporting Information

Supporting Information Available:

Theoretical detailed calculation of the TENG equivalent circuit, the shrunk TENG signal width under 1 kΩ, 100 kΩ and 100 MΩ external load and the detailed reason for the resonant frequency fluctuation of the TENG-inductor circuit.(PDF)

Supporting video

Movie S1: The sensing system wireless transmit light signal to 3 meters away. (MP4)

Movie S2: The sensing system wireless transmit light signal to photodiode and the following amplifier, and then it is displayed on oscilloscope. (MP4)

Author contributions

J. Chen and W.Xuan designed, fabricated and characterized the TENG wireless sensors, P.Zhao U.Farooq and P.Ding, assisted the fabrication and characterization of the TENG sensor devices, and data analysis, W.Yin, H.Jin, X.Wang, Y. Fu, S.Dong and J.Luo contributed the ideas and suggestions for the development, preparation of the paper. All authors participated discussions during the research and preparation of the paper.

Acknowledgements

Project was supported by NSFC (Nos. 61301046, 61376118, U1613202 and U1609210) and “the Fundamental Research Funds for the Central Universities 2016XZZX001-05”. The authors also acknowledge the Innovation Platform of Micro/Nanodevices and Integration System, Zhejiang University. Jinkai Chen acknowledges the Graduate Education International Exchange Fund from Zhejiang University for sponsoring his study at the University of Manchester.

References

[1] J. Gubbi, R. Buyya, S. Marusic, M. Palaniswami, Future Gener. Comp. Sy., 29 (2013) 1645-1660.

[2] D. Silver, A. Huang, C.J. Maddison, A. Guez, L. Sifre, G. van den Driessche, J. Schrittwieser, I. Antonoglou, V. Panneershelvam, M. Lanctot, S. Dieleman, D. Grewe, J. Nham, N. Kalchbrenner, I. Sutskever, T. Lillicrap, M. Leach, K. Kavukcuoglu, T. Graepel, D. Hassabis, Nature, 529 (2016) 484.

[3] J. Davis, T. Edgar, J. Porter, J. Bernaden, M. Sarli, Comput. Chem. Eng., 47 (2012) 145-156.

[4] S. Wang, X. Wang, Z.L. Wang, Y. Yang, Acs Nano, 10 (2016) 5696-5700.

[5] L. Jin, W. Deng, Y. Su, Z. Xu, H. Meng, B. Wang, H. Zhang, B. Zhang, L. Zhang, X. Xiao, M. Zhu, W. Yang, Nano Energy, 38 (2017) 185-192.

[6] Y. Fan, G. Zhong, J. Cheng, L. Songwu, Z. Lixia, 23rd International Conference on Distributed Computing Systems, 2003. Proceedings.2003, pp. 28-37.

[7] R.G. Azevedo, D.G. Jones, A.V. Jog, B. Jamshidi, D.R. Myers, L. Chen, X.a. Fu, M.

Mehregany, M.B.J. Wijesundara, A.P. Pisano, IEEE Sens. J., 7 (2007) 568-576.

[8] Y. Wang, Y. Jia, Q. Chen, Y. Wang, Sensors, 8 (2008).

[9] K. Zhao, Z.L. Wang, Y. Yang, Acs Nano, 10 (2016) 9044-9052.

[10] R.A. Steven, A.S. Henry, Smart Mater. Struct., 16 (2007) R1.

[11] K.A. Cook-Chennault, N. Thambi, A.M. Sastry, Smart Mater. Struct., 17 (2008) 043001.

[12] Y. Yang, W. Guo, K.C. Pradel, G. Zhu, Y. Zhou, Y. Zhang, Y. Hu, L. Lin, Z.L. Wang, Nano Lett., 12 (2012) 2833-2838.

[13] C.R. Bowen, J. Taylor, E. LeBoulbar, D. Zabek, A. Chauhan, R. Vaish, Energ. Environ. Sci., 7 (2014) 3836-3856.

[14] A.R.M. Siddique, S. Mahmud, B.V. Heyst, Energy Convers. Manage., 106 (2015) 728-747.

[15] S.P. Beeby, R.N. Torah, M.J. Tudor, P. Glynne-Jones, T.O. Donnell, C.R. Saha, S. Roy, J. Micromech. Microeng., 17 (2007) 1257.

[16] Z.L. Wang, Acs Nano, 7 (2013) 9533-9557.

[17] G. Zhu, Z.-H. Lin, Q. Jing, P. Bai, C. Pan, Y. Yang, Y. Zhou, Z.L. Wang, Nano Lett., 13 (2013) 847-853.

[18] Z.L. Wang, Faraday Discuss., 176 (2014) 447-458.

[19] W. Shuhua, M. Xiaojing, Y. Ya, S. Chengliang, G.A. Yuandong, W.Z. Lin, Adv. Mater., 27 (2015) 240-248.

[20] Y. Yang, H. Zhang, X. Zhong, F. Yi, R. Yu, Y. Zhang, Z.L. Wang, Acs Appl. Mater. Inter., 6 (2014) 3680-3688.

[21] B. Zhang, L. Zhang, W. Deng, L. Jin, F. Chun, H. Pan, B. Gu, H. Zhang, Z. Lv, W. Yang,

Z.L. Wang, Acs Nano, 11 (2017) 7440-7446.

[22] F.-R. Fan, Z.-Q. Tian, Z. Lin Wang, Nano Energy, 1 (2012) 328-334.

[23] W. Shuhua, W.Z. Lin, Y. Ya, Adv. Mater., 28 (2016) 2881-2887.

[24] X. Wang, S. Wang, Y. Yang, Z.L. Wang, Acs Nano, 9 (2015) 4553-4562.

[25] Z. Kewei, W. Shuhua, Y. Ya, Adv. Energy Mater., 7 (2017) 1601852.

[26] T. Quan, X. Wang, Z.L. Wang, Y. Yang, Acs Nano, 9 (2015) 12301-12310.

[27] Y. Yang, Z.L. Wang, Nano Energy, 14 (2015) 245-256.

[28] L. Jin, J. Chen, B. Zhang, W. Deng, L. Zhang, H. Zhang, X. Huang, M. Zhu, W. Yang, Z.L. Wang, Acs Nano, 10 (2016) 7874-7881.

[29] B. Zhang, J. Chen, L. Jin, W. Deng, L. Zhang, H. Zhang, M. Zhu, W. Yang, Z.L. Wang, Acs Nano, 10 (2016) 6241-6247.

[30] K. Myny, S. Steudel, S. Smout, P. Vicca, F. Furthner, B. van der Putten, A.K. Tripathi, G.H. Gelinck, J. Genoe, W. Dehaene, P. Heremans, Org. Electron., 11 (2010) 1176-1179.

[31] C.S. Hartmann, 2002 IEEE Ultrasonics Symposium, 2002. Proceedings.2002, pp. 65-69 vol.61.

[32] V.P. Plessky, L.M. Reindl, IEEE T. Ultrason. Ferr., 57 (2010) 654-668.

[33] S. Niu, S. Wang, L. Lin, Y. Liu, Y.S. Zhou, Y. Hu, Z.L. Wang, Energ. Environ. Sci., 6 (2013) 3576-3583.

[34] J. Chen, H. Guo, P. Ding, R. Pan, W. Wang, W. Xuan, X. Wang, H. Jin, S. Dong, J. Luo, Nano Energy, 30 (2016) 235-241.

[35] R.D.I.G. Dharmasena, K.D.G.I. Jayawardena, C.A. Mills, J.H.B. Deane, J.V. Anguita, R.A.

Dorey, S.R.P. Silva, Energ. Environ. Sci., 10 (2017) 1801-1811.

[36] S. Niu, Y.S. Zhou, S. Wang, Y. Liu, L. Lin, Y. Bando, Z.L. Wang, Nano Energy, 8 (2014) 150-156.

[37] N. Soin, P. Zhao, K. Prashanthi, J. Chen, P. Ding, E. Zhou, T. Shah, S.C. Ray, C. Tsonos, T. Thundat, E. Siores, J. Luo, Nano Energy, 30 (2016) 470-480.

[38] P. Ding, J. Chen, U. Farooq, P. Zhao, N. Soin, L. Yu, H. Jin, X. Wang, S. Dong, J. Luo, Nano Energy, 46 (2018) 63-72.

[39] G. Cheng, Z.-H. Lin, L. Lin, Z.-l. Du, Z.L. Wang, Acs Nano, 7 (2013) 7383-7391.

[40] P. Vasandani, B. Gattu, Z.-H. Mao, W. Jia, M. Sun, Nano Energy, 43 (2018) 210-218.

[41] L.S. McCarty, G.M. Whitesides, Angew. Chem. Int. Edit., 47 (2008) 2188-2207.